




Article

# On the Hybridization of Microcars with Hybrid UltraCapacitors and Li-Ion Batteries Storage Systems

Fernando Ortenzi <sup>1,\*</sup> , Natascia Andrenacci <sup>1</sup> , Manlio Pasquali <sup>1</sup> and Carlo Villante <sup>2</sup> 

<sup>1</sup> ENEA—Italian Agency for New Technologies, Energy and Sustainable Economic Development, 00134 Rome, Italy; natascia.andrenacci@enea.it (N.A.); manlio.pasquali@enea.it (M.P.)

<sup>2</sup> CITraMS—Center for Transportation and Sustainable Mobility, University of L'Aquila, 67100 L'Aquila, Italy; carlo.villante@univaq.it

\* Correspondence: fernando.ortenzi@enea.it; Tel.: +39-06-3048-6184

Received: 19 May 2020; Accepted: 18 June 2020; Published: 22 June 2020



**Abstract:** The objective proposed by the EU to drastically reduce vehicular CO<sub>2</sub> emission for the years up to 2030 requires an increase of propulsion systems' efficiency, and accordingly, the improvement their technology. Hybrid electric vehicles could have a chance of achieving this, by recovering energy during braking phases, running in pure electric mode and allowing the internal combustion engine to operate under better efficiency conditions, while maintaining traditionally expected vehicle performances (mileage, weight, available on-board volume, etc.). The energy storage systems for hybrid electric vehicles (HEVs) have different requirements than those designed for Battery Electric Vehicles (BEVs); high specific power is normally the most critical issue. Using Li-ion Batteries (LiBs) in the designing of on-board Energy Storage Systems (ESS) based only on power specifications gives an ESS with an energy capacity which is sufficient for vehicle requirements. The highest specific power LiBs are therefore chosen among those technologically available. All this leads to an ESS design that is strongly stressed over time, because current output is very high and very rapidly varies, during both traction and regeneration phases. The resulting efficiency of the ESS is correspondingly lowered, and LiBs lifetime can be relevantly affected. Such a problem can be overcome by adopting hybrid storage systems, coupling LiBs and UltraCapacitors (UCs); by properly dimensioning and controlling the ESS' components, in fact, the current output of the batteries can be reduced and smoothed, using UCs during transients. In this paper, a simulation model, calibrated and validated on an engine testbed, has been used to evaluate the performances of a hybrid storage HEV microcar under different operative conditions (driving cycles, environment temperature and ESS State of Charge). Results show that the hybridization of the powertrain may reduce fuel consumption by up to 27%, while LiBs lifetime may be more than doubled.

**Keywords:** microcars; hybrid vehicles; hybrid storage; Li-Ion Battery; UltraCapacitors

## 1. Introduction

Mobility in modern metropolitan cities, especially within historical city centers, is affected by overcrowding, congestion, low transit speed, fuel consumption, air pollution and parking problems. Among the causes of these phenomena, there is the diffusion of vehicles of excessive size with respect to their use, and the low occupancy rate of vehicles. Indeed, according to a study from the National Association of Italian Municipalities (ANCI) [1–3], 66% of the vehicles are occupied only by the driver, with an average of 1.33 passengers per vehicle.

Furthermore, the Italian Higher Education and Research Institute for Transport (ISFORT) in 2018 published a study about the distribution of travelled distances per capita in Italy; 76.5% of the distances were below 10 km, as reported in Table 1.

**Table 1.** Distribution of shift for different distances, ISFORT 2018 [2].

Distance	%
<2 km	33.2
2–10 km	43.3
10–50 km	19.8
>50	2.8

A possible solution to such a transport demand, especially in big cities, could be the adoption of microcars. These vehicles have the advantages of low weight, low power and traction energy demands over common vehicles, and are suitable in urban environments where the average speeds are low.

The EU normatively groups these little vehicles into a category called “quadricycles”, which could be “Light” and “Heavy”. To be homologated as a Heavy quadricycle, a vehicle should have these characteristics:

- maximum speed  $\leq 90$  km/h (45 km/h for Light quadricycles)
- mass in running order  $\leq 450$  kg (350 kg for Light quadricycles)
- continuous rated maximum power  $\leq 15$  kW (4 kW for Light quadricycles).

Many models of this type are present on the EU market. They do not require a driving license and have a very low fuel consumption (normally  $< 3$  L/100 km). All these characteristics make these vehicles particularly attractive in urban context (especially in very narrow and hard-to-traverse EU historical city centers), and offer a substantial contribution to the very restrictive EU objectives in terms of CO<sub>2</sub> emission reductions from transport.

To this end, a relevant increase is required in terms of propulsion systems efficiency; Hybrid Electric Vehicles (HEVs) have a chance of achieving this, by recovering energy during braking phases, running in pure electric mode and allowing the internal combustion engine to operate under better efficiency conditions, while maintaining traditionally expected vehicle performances (mileage, weight, available on-board volume, etc.).

Hybridization is one of the most efficient technologies for reducing CO<sub>2</sub> from vehicles. Microcars can benefit from the adoption of hybrid powertrains; in [4], a reduction of about 20% in fuel consumption was obtained with the addition of a little electric motor to the powertrain of the vehicle. The addition of a second source of power can allow the internal combustion engine to run at its highest efficiency points, increasing the global efficiency of the powertrain [5].

Energy Storage Systems (ESS) for HEVs have different requirements than those designed for battery electric vehicles (BEVs), and high specific power is normally the most critical issue. When using Li-ion Batteries (LiBs) in designing on-board ESS based only on power specifications, an energy capacity which is sufficient for the vehicle’s requirements can be achieved. Highest specific power LiBs are therefore chosen among those technologically available. All this leads to an ESS design which is strongly stressed over time, because current output is very high and very rapidly varies, during both traction and regeneration phases. The resulting efficiency of the ESS is correspondingly lowered, and LiBs lifetime can be relevantly affected.

Such a problem can be overcome by adopting a hybrid ESS, and coupling energy designed storages with power designed ones is the most common application. For example, the coupling of a lead acid battery with UltraCapacitors (UCs) is reported in [6–8]. The UCs, with their high specific power, increase the total performance and the battery life. In [6], the lead acid battery life was more than doubled and the range of the microcar increased more than 46%, while in [7] no advantages in terms of range were observed when batteries were used with a simple parallel to join the two sources of energy. The simple parallel (passive mode), however, is not the best solution for coupling batteries and UCs, since the UCs are used in a limited portion of their available State of Charge (SOC), leading to an over-dimensioning of the UCs’ branch of the ESS.

The addition of an inductance in series with the battery [9] can improve voltage (and correspondently SOC) oscillations at the UCs output, limiting power transients in the battery and

increasing its lifetime. In hybrid ESS, in fact, an increased battery life can be observed, both in BEVs [10] and in HEVs [10] applications, according to various hybrid ESS design approaches. These, as already introduced, could vary widely, ranging from the simplest option of a parallel connection, up to the more complex but better-performing introduction of a DC/DC converter at the UCs branch [10–12].

It is here important also to go deeper in the discussion about battery lifetime, it being one of the most critical problems connected with BEVs and HEVs development. Battery aging represents the result of an internal degradation phenomena. Since the internal processes of the battery can be non-linear, the evolution of battery degradation over time depends in a non-trivial way on the conditions of use or storage, as well as on the specific cell construction technology [13]. In general, aging is classified under:

- Calendar life, which is linked to intrinsic degradation under conditions of non-use, and is therefore a function of time (as well as storage conditions).
- Cycle life, linked to the use of the battery in certain work cycles. In this case, the lifespan can be expressed with respect to various parameters, such as time, the number of cycles, the total capacity supplied by the battery, etc.

Battery degradation is essentially measured through a progressive loss of capacity and an increase in the internal resistance, which leads to a decrease in the power supplied. The fact that performance losses are progressive poses the problem of the definition of end-of-life (EOL) for LiBs. In automotive applications, a 20–30% decrease in capacity compared to the initial value, or a doubling of the value of the internal resistance (IR), is commonly accepted as the EOL criterion ISO 12405–2 [14].

Regarding battery aging modeling and prediction, there are different approaches to tackle the problem; even if there is no official classification, and some approaches can be hybrid, they can be divided in three categories:

- Electrochemical models describe the battery starting from the physical phenomena that take place inside it. These models are very complex, and are described by systems of coupled differential equations with a large number of parameters.
- In analytical models, the battery is represented by a few equations that reproduce certain responses to given stimuli. In particular, these models correlate the stresses to which the battery is subjected with the trend of key quantities, such as capacity and internal resistance; the estimation of the aging parameters is done based on experimental measurements.
- Statistical approaches rely heavily on experimental data to predict battery behavior, and often they do not rely on any physical considerations. An example of statistical approach is the Autoregressive Moving Average (ARMA), which uses time series to deduce the aging level. Particle filtering is another possible statistical approach that can predict the trend of battery degradation.

All this considered, a HEV microcar (a Heavy quadricycle according to EU directives), named “Spazia”, was designed, realized and tested in the ENEA Facility [15]. Basing on experimental data regarding this vehicle, a calibrated and validated vehicle simulation model was obtained, including a model for the ICE (Internal Combustion Engine) called EngineSim [16,17] and for the centrifugal CVT (Continuously Variable Transmission) [4]. A model was used to evaluate expected vehicle fuel consumption and emissions, for a range of different operative conditions.

Based on the results of this modeling activity, the HEV microcar was analyzed, optimized and redesigned in all its main components, in order to better position the vehicle within the EU Heavy quadricycles category, reaching 15 kW of maximum power. Then, a proper control strategy for the HEV propulsion system was proposed and tested, in order to maximize the fuel consumption reduction.

Analyses have been performed regarding both conventional (LiBs-based) ESS and hybrid (LiBs and UCs) ESS, which have been tested and compared over several driving cycles, such as FTP75, WLTC Class 1 and Artemis Urban.

During the simulations, a model for battery aging was used [10,18], in order to mimic their degradation (until they reached the end of their life; that is, 80% of the remaining capacity) and compare the LiBs cycle life between the two configurations.

## 2. Vehicle Specification

The present work starts from a previous experimentation, performed at the ENEA Research Centre, on the existing chassis of a quadricycle called ERAD SPAZIA (born as a Lead Acid BEV), which was then converted to a parallel HEV by installing a Hybrid Powertrain Pack (HPP). Such a vehicle was tested on a rolling dynamometer chassis, and each of its main components were separately and extensively tested on dedicated test benches (see Figure 1). For a complete description of these activities, please refer to [15,19].

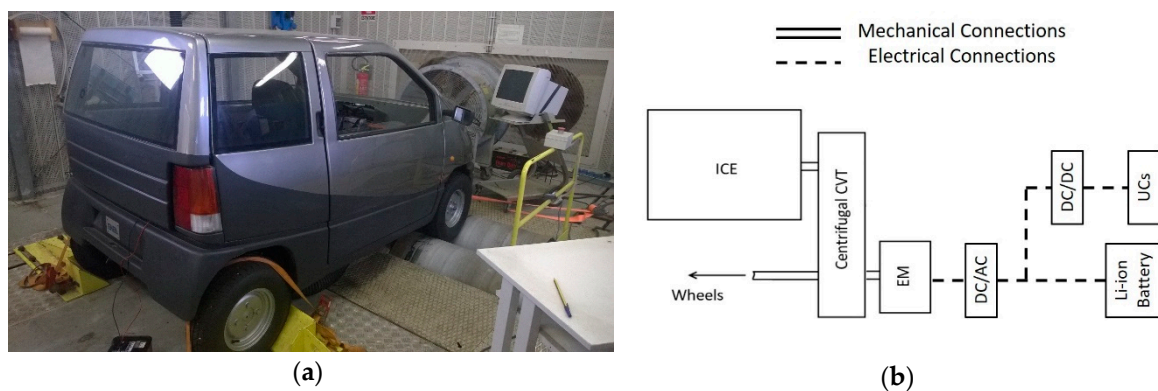


Figure 1. (a) Erad Spazia Quadricycle; (b) the hybrid powertrain scheme [15].

The vehicle is now a hybrid heavy quadricycle, with an ICE hybridized with a permanent magnet electric motor mounted on the secondary axis of its centrifugal continuously variable transmission (CVT). The vehicle's total weight is 550 kg, which is the maximum allowed weight of the Heavy quadricycles (450 kg, plus the driver, fuel, etc., for an additional weight of 100 kg). Its frontal area and the drag coefficient were measured during coast-down tests, subtracting from the total deceleration force the tires' friction resistances, and the results are reported in Table 2.

Table 2. Specification.

Weight	550 kg
Drag Coefficient	0.335
Frontal area	2 m <sup>2</sup>
Auxiliaries	200 W
Wheels radius	0.26 m
ICE Model	Lombardini 442 CRS
ICE max power	8.5 kW @ 4300 Rev/min
Transmission ratio	With CVT: 0.5–2
Electric Motor	Heinzmann PMS100
Inverter	Sevcon Gen4
Nominal Voltage	48 V
Rated Power (Torque)	2.7 kW (4.3 Nm)
Maximum Power (Torque)	6.7 kW (20 Nm)
Rated speed	6000 Rev/min
Final gear ratio	10

The measured auxiliaries consumption was about 200 W, comparable with that measured on a recent diesel microcar, as in [17]. However, in this HEV configuration, auxiliaries may be directly supplied by the vehicle's DC bus for ESS and traction motor purposes. This option, in fact, showed a

better efficiency than connecting them with the pre-existing on-board alternator (connected to the ICE crankshaft via a dedicated belt, with a global efficiency of about 60%). This resulted in both a non-negligible reduction of consumption and the removal of the 12 V alternator, as well as the 12 V Pb-Acid battery normally dedicated to the auxiliaries' supply. By this approach, the ESS energy requirements for the HPP increased, which makes it impossible to think of an ESS made with UCs only.

The ICE is a Lombardini 442 CRS (in Table 2), whose maximum power is 8.5 kW at 4300 Rev/min (power was increased with respect to a previously experimented HPP by the same authors, dedicated to light quadricycles: 4 kW at 3600 Rev/min [4,15]). Its centrifugal CVT has a transmission ratio from 0.5 to 2, continuously varying as a function of the engine Rev/min and torque, which was fully experimentally characterized. The derivation of a physically consistent dedicated model of the CVT was the main object of a previous publication by the same authors, and is fully detailed in in [4].

Dedicated experimental activities on an ICE test bench permitted us to derive an ICE fuel consumption map to be used in vehicle simulations (see Figure 2). Due to the restriction imposed on the power output of the experimented version of the ICE, the highest part of the map has been built using an engine simulation model called EngineSim, validated with any possible measurement on the real engine (which was limited to a power output of 4 kW).

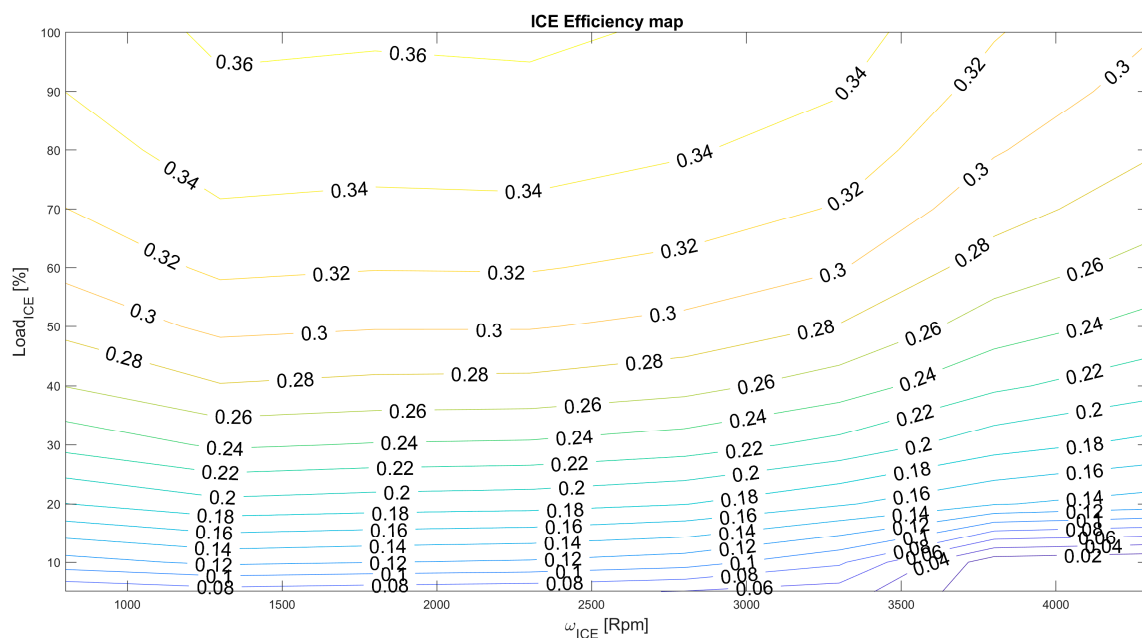


Figure 2. ICE map efficiency vs Rev/min and Load%.

The electric motor is the Heinzmann PMS100 48 V, with a rated power of 2.7 kW and a Peak Power of 6.7 at 6000 Rev/min [20]. The inverter is the Gen4 from SEVCON.

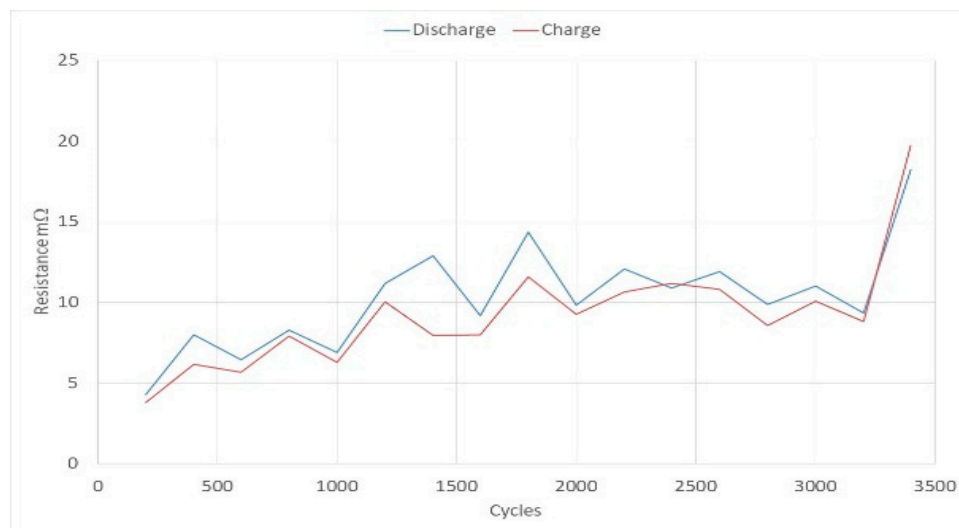
As previously underlined, the design was chosen to connect the electric motor to the secondary axis of the CVT, so that the vehicle can also run in electric mode, if needed, for limited durations according to the capacity of the ESS [15].

A hybrid ESS was used, coupling LiBs and UCs through a dedicated DC/DC converter. The LiBs' specifications are reported in Table 3: 13 NMC (Nickel Manganese Cobalt) 20 h cells manufactured from EIG in series have been used, with 48 V of nominal voltage and a total energy of 0.77 kWh.

**Table 3.** Specification.

Onboard Battery	
EIG NMC Cell Capacity	20 Ah
Nominal Voltage	3.7 V
Discharge C Rate	5C/(10C)
Continuous/(peak)	
Charge C RateContinuous/(peak)	2C/(5C)
Cells in series	13
Nominal Voltage	48.1 V
Energy stored	0.77 kWh

Their maximum continuous discharge current is 100 A (at 5C rate); peaks of 200 A (10C rate) are possible for periods shorter than 10 s, which is normally within typical specifications for HEVs applications. Further cell characteristics used in the simulations (internal resistance, capacity and open circuit voltage) are those measured at the end of their life, at 80% of their capacity (see also Figure 3).

**Figure 3.** Internal resistance variation with aging for SOC (State of Charge) = 50%.

The UCs used are the Maxwell 16 V and 250F modules [7]; they have a high specific power together with a long life compared to the batteries, but on the other hand, their specific energy is quite low (2.11 Wh/kg vs 174 Wh/kg of the EIG Cells) (see Figure 4). The advantage of adopting a hybrid storage is that the UCs help the LiBs during the high-power phases, also preserving their health. Practically, the addition of UCs increases the specific power and the cycle life of the battery. To connect the UCs with the LiBs, and to allow a control strategy between the two sources of energy, a DC/DC converter has been used, as in [8,10,19].



Maxwell	UCs
Capacitance	250 F
Nominal Voltage	16 V
Maximum Current	1000 A
Internal Resistance	4.1 mΩ
Modules in Series	2
Energy Stored	17.8 Wh
Life at 25°C	10 years–10 <sup>6</sup> Cycles

**Figure 4.** BMOD0500 P016 B02 modules specification.

Among the possible alternative options [10], the simplest one was to connect the LiBs directly in parallel with the UCs, without any DC/DC converter, as in Figure 5 [7,21], but the UCs could not be used at their maximum potentialities. In this latter design option, in fact, current (and power) split between UCs and LiBs would be a simple consequence of the internal resistances of the two branches, and no power-split control strategy would be applicable. A possible correction of the resulting behavior (but still without any active control of the power-split) could be obtained through the insertion of a properly dimensioned inductance in series with the LiBs [9], which could increase UCs usage.

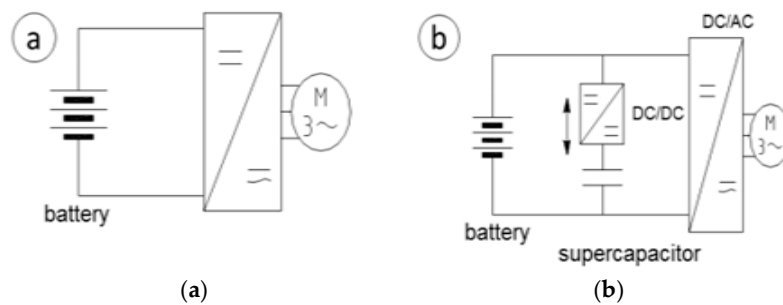


**Figure 5.** Architectures for the hybrid storage: (a) Battery Based; (b) Hybrid ESS solution

The designed UCs consists of two modules with an overall nominal voltage of 32 V, which is lower than the nominal voltage of the LiBs branch; therefore, the DC/DC converter works in “Buck” mode when supplying power to the electric motor, and in boost mode when recovering energy. The efficiency curve of the converter was experimentally measured with dedicated equipment in a previous research activity for other purposes [12], and is reported in Figure 6.

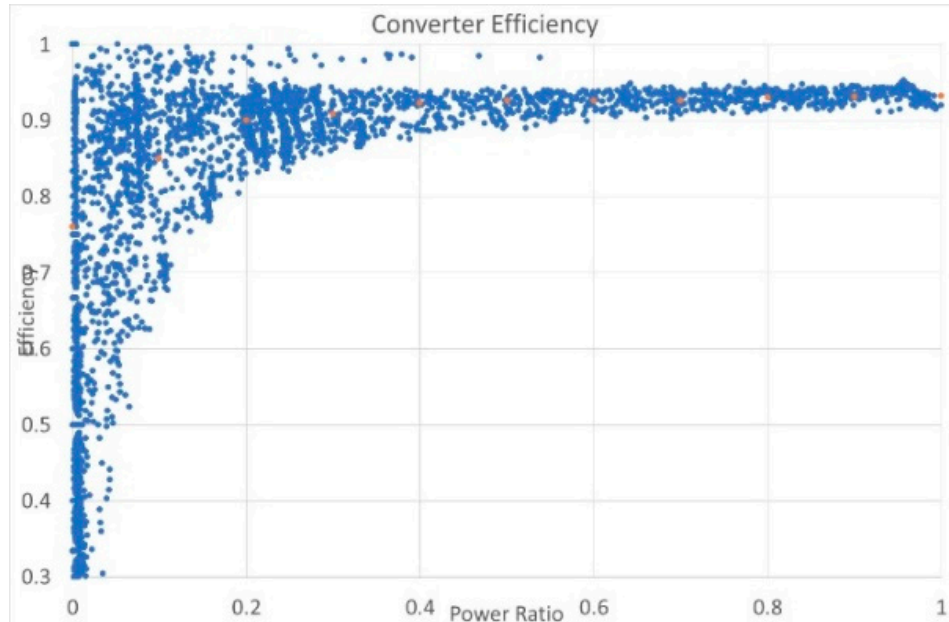


**Figure 6.** Efficiency of the DC/DC converter.

### 3. HPP Control Strategy

The hybrid control strategy presented in the present work is a part of the numerical models used to calculate the engine maps (EngineSim) and the fuel consumption of vehicles running driving cycles (VehicleSim).

EngineSim is an in-house code written in Visual Basic that simulates engines in all the components [16,17]; it uses 1D models to simulate the manifolds (second order Upwind Hancock

model [22]) and their pipe bounds, like junctions, valve boundaries, throttles and open ends, a quasi-dimensional two zone combustion model and zero-dimensional model for plenums.

An in-house numerical code (named VehicleSim, see [4,17] for reference) that calculates the fuel consumption of a specified vehicle running a driving cycle (in Figure 7 the cycles used are reported) has been developed, and here used to compute WLTC Class 1, Artemis Urban and FTP75 driving cycles, using the data from the selected vehicles and engines. The instantaneous value of power in a driving cycle is calculated as the sum of slope, aerodynamic and friction losses; the transmissions are simulated with their transmission ratio and efficiencies, and the electric motor and the internal combustion engine are simulated using 3D maps with rpm and torque.

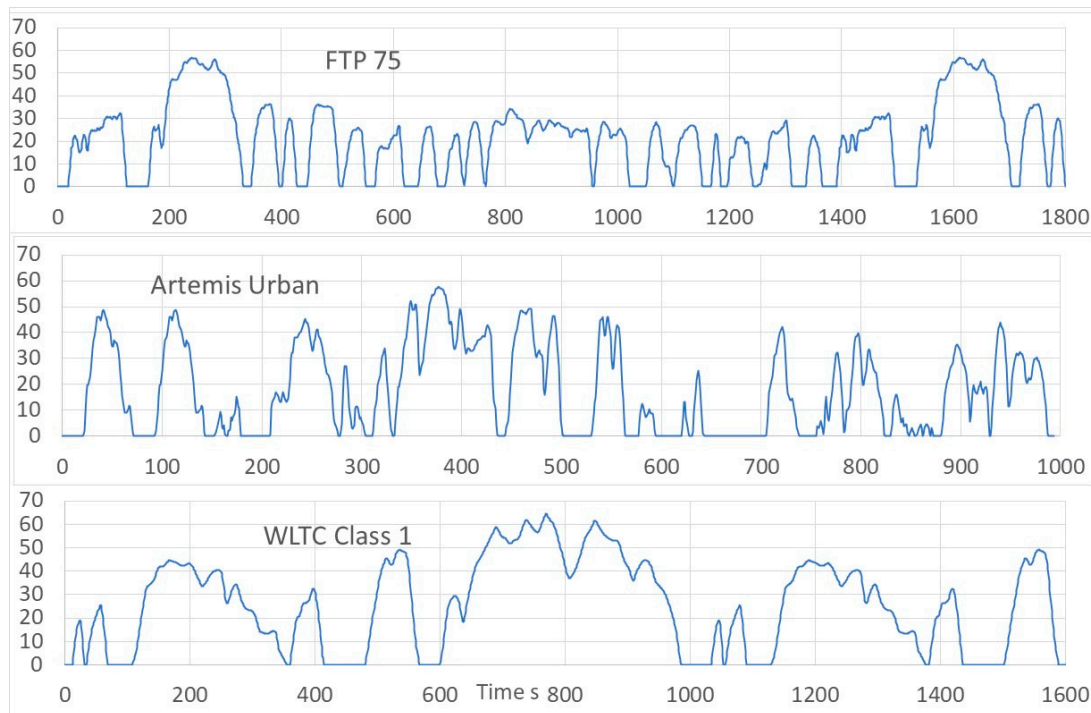


**Figure 7.** Driving cycles used during the simulations: WLTC Class 1, FTP75 and Artemis Urban.

The battery's State of Charge is calculated as the integral of the instantaneous current:

$$SOC_b = SOC_{b0} - \frac{\int I \cdot \frac{dt}{3600}}{Ah_b} \quad (1)$$

with  $SOC_{b0}$  as the State of Charge at the start of the simulation,  $Ah_b$  battery capacity expressing ampere/hour.

The UltraCapacitors' SOC is instead calculated as:

$$SOC_{UC} = SOC_{UC0} - \frac{\int I \cdot dt - C_{UC} \cdot V_{min}}{C_{UC} \cdot (V_{max} - V_{min})} \quad (2)$$

With  $C_{UC}$  as the capacity, expressed in Farad;  $V_{max}$  is the maximum voltage, and in the present work is the nominal voltage.  $V_{min}$  is the minimum voltage, and is  $\frac{V_{max}}{2}$ .

With Equation (2), the UltraCapacitors have  $SOC = 1$  when the voltage is  $V_{max}$ , and is  $SOC = 0$  when the voltage is  $V_{min}$ .

The main purpose of adopting a hybrid powertrain is to reduce the fuel consumption of the thermal engines, and to lower ICE transients and corresponding pollutant emissions. Therefore, the HPP control strategy was designed with the following objectives:



- To optimize HPP global efficiency, making ICE work around its best possible efficiency points
- To optimize energy recovery in deceleration phases
- To make it possible, if needed, to run in electric mode at low speed.

In Figure 8, the calculated global efficiency for the vehicle is reported in steady conditions, as a function of required wheel power and electric motor power output.

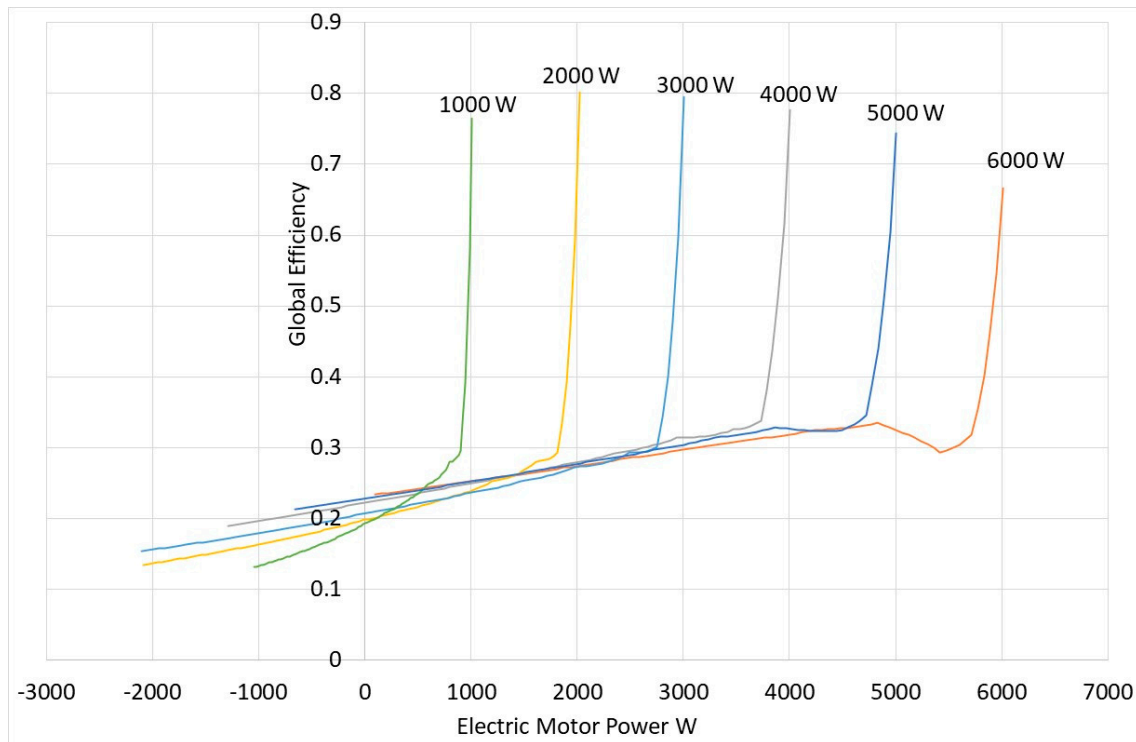


**Figure 8.** Efficiency of the powertrain for different wheel power values (from 1000 W to 6000 W) and different values of electric motor power.

This considers the efficiencies of all the components involved (ICE, electric motor, transmission and ESS) according to the following formulation [5]:

$$\eta_t = \frac{P_{Wheel}}{P} = \frac{P_{Wheel}}{P_{Fuel}^{ICE} + P^{Batt}} \quad (3)$$

According to Figure 8, moving rightwards on each of the represented curves, the vehicle is using electric energy for traction purposes to increasing extents (up to pure electric drive conditions), instead of using diesel fuel. Obviously, the efficiency being based on a steady Tank-to-Wheels (TTW) approach, all the curves have their maximum values when the vehicle runs in electric mode (when the ICE power = 0, the efficiency is between 0.7 and 0.8) and decrease rapidly when the internal combustion engine power is increased (up to 0.14, and generally between 0.2 and 0.3). When the electric power is negative (the ICE is used for traction and also to charge the batteries), the efficiency values are the lowest, and decrease if the requested wheel power is decreased.

Obviously, the electric mode is therefore the most efficient condition on a TTW basis: the controller should therefore maximize the amount of energy given to the wheels in an electric way, controlling the availability of electric energy in the hybrid ESS, also leaving available space, in terms of ESS State of Charge (SOC), in order to implement regenerative vehicle deceleration.

To this end, various possible algorithms are possible. Some of these were already presented and discussed by the authors in [4]. Here, the best control algorithm selected in [4] was applied with some further modifications, finally gaining the following control rules:

- If the wheel torque is lower than a threshold value, the vehicle runs in electric mode; generally, this happens at low or constant speeds and for negative torque values, when the electric motor recovers energy. This phase is of maximum efficiency.
- The threshold value is a fraction (0 to 1) of the maximum available thermal engine torque at the actual Rev/min.
- For higher values of wheel torque, the vehicle runs in hybrid mode. The optimum point can be found in Figure 8, and a strategy to find the best value can be developed. A simpler, but equally efficient, strategy can be developed using the vehicle in electric mode as much as possible, and when in hybrid mode using a part of the available power to charge the batteries and restore the battery's SOC. In this way, the engine runs at higher loads, where there are the highest values of efficiency.

The ICE torque is then calculated as follows:

$$T_{Wheel}^{ICE} = \begin{cases} 0 \rightarrow T_{Wheel} \leq C_{el} \cdot T_{ICE}^{Max}(Rpm) \\ T_{Wheel} + T_{Charge} \rightarrow T_{wheel} \geq C_{el} \cdot T_{ICE}^{Max}(Rpm) \end{cases} \quad (4)$$

where  $T_{Wheel}^{ICE}$  is the internal combustion engine's wheel torque,  $T_{Wheel}$  is the total requested wheel torque,  $T_{ICE}^{Max}(Rpm)$  is the maximum ICE torque at a specified Rev/min,  $C_{el}$  is a control coefficient variable with SOC (increasing with SOC),  $T_{Charge}$  is the additional torque by the ICE for ESS charging purposes, and  $T_{Charge}$ , on its turn, may be calculated as a function of the available ICE torque:

$$T_{Charge} = C_{Charge} \cdot (T_{ICE}^{Max} - T_{wheel}) \quad (5)$$

Its value is a function of the residual torque available at ICE shaft ( $T_{ICE}^{Max} - T_{wheel}$ ) through a control coefficient  $C_{Charge}$  (decreasing with SOC).

In the designed controller, the two control coefficients were imposed to vary linearly, with the LiBs SOC ( $SOC_b$ ) ranging from 0 to their maximum values, according to the following equations:

$$C_{el} = C_{el0} \cdot f_{el}(SOC_b) \quad (6)$$

$$C_{Charge} = C_{Charge0} \cdot f_{Charge}(SOC_b) \quad (7)$$

Both  $f_{el}$  and  $f_{Charge}$  have been reported in Figure 9, and their values vary, for the maximum and minimum values of SOC, between 0.3 and 0.7 (with an average value of 0.5); the typical range for the optimal use of batteries.

This results in an auto-tunable model in which, if the driving cycle has low electric power request (and the SOC increases), the  $C_{el}$  value increases and the  $C_{Charge}$  decreases, and the contrary is true with decreasing battery SOC.

The model can be calibrated with two coefficients: in the present work with the engine, we used  $C_{el0} = 0.5$  and  $C_{Charge0} = 0.5$ .

The input data of the model are then: (I) the requested wheel torque, (II) the maximum engine torque at the actual engine rpm, and (III) the actual battery SOC. The output are: (I) the internal combustion engine wheel torque, and (II) the electric motor wheel torque.

During simulations, the initial and final battery SOC levels were deduced to be the same, in order to calculate the real fuel consumption without storing or extracting additional energy from the battery.

Simulations were made with the vehicle running on the WLTC homologation cycle, imposed by the EU directives for this category of vehicles.

The benefits of adopting hybrid powertrains are shown in Figure 10; for lower values of power, the vehicle runs in electric mode, while at higher ones the engine supplies more power to charge the battery too (in Figure 10). In this way, the engine can work at higher loads, typically with higher efficiency.

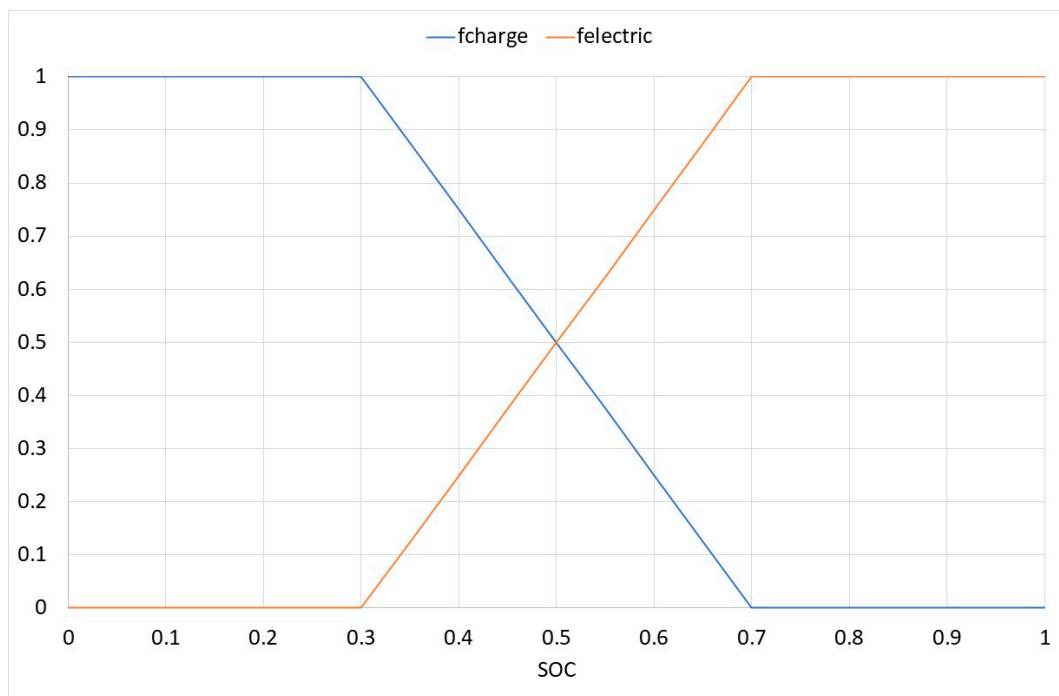


Figure 9.  $f_{Charge}(SOC_b)$  and  $f_{el}(SOC_b)$  values with SOC.

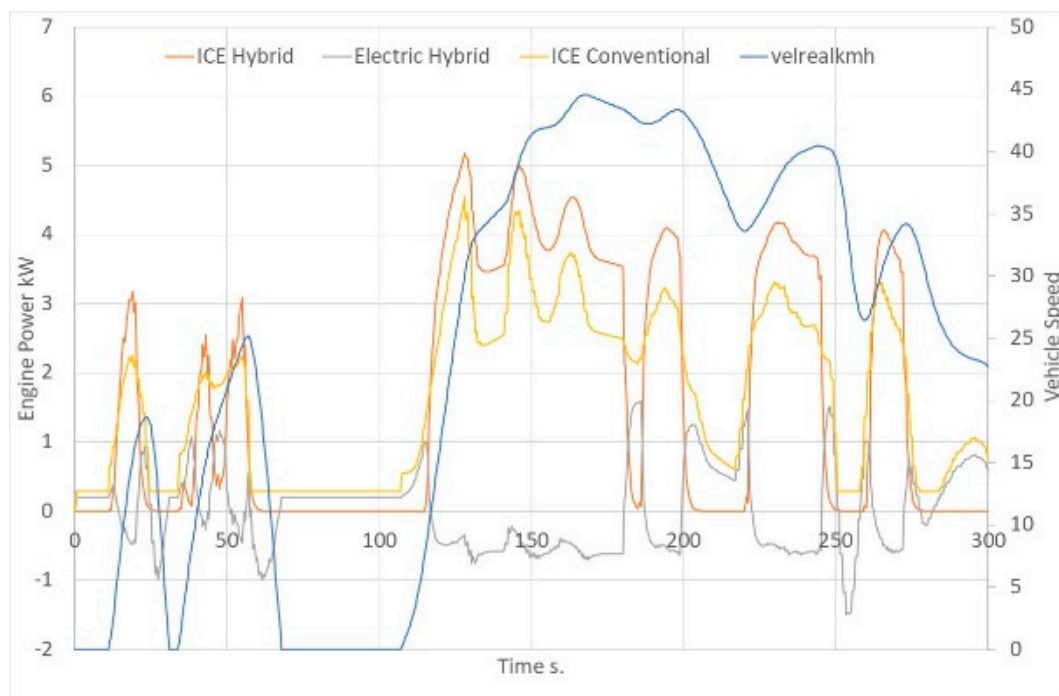
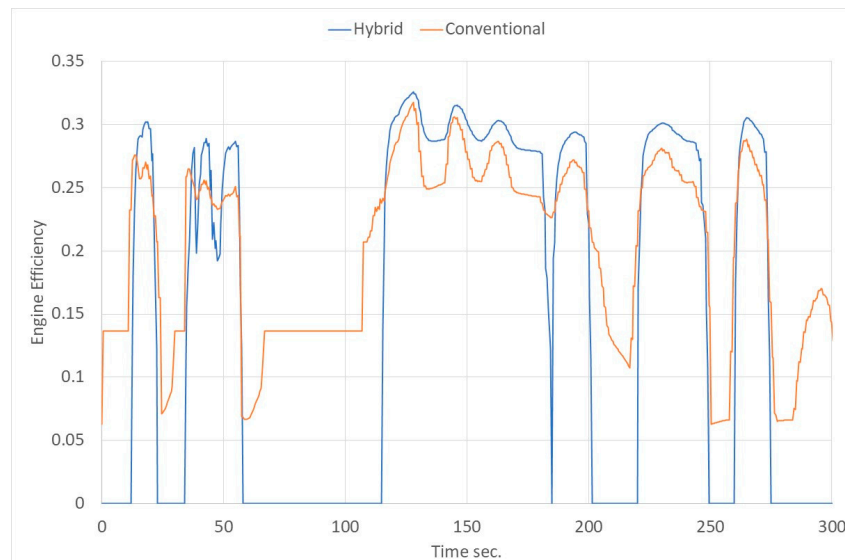


Figure 10. Power output at ICE and electric motor for conventional and hybrid powertrain.

Figures 10 and 11 make it possible to shed light on some important behaviors of the vehicle:

- The stop and start phases (for example, between 70 and 120 s), with the internal combustion engine off and the auxiliaries supplied by the electric subsystem
- The regenerative braking phases (around 250 s), where the battery is charged by the electric motor, then energy recovery during the braking phase

- The electric mode phases (200–220 s), at low speed and low load, where the internal combustion engine is off, and the vehicle is moved by the electric motor
- The phases where the internal combustion engine supplies power to the vehicle and also to charging the battery (120–180 s). Such phases are at high efficiency, as shown in Figure 11.



**Figure 11.** Efficiency of ICE running the WLTC Class 1 driving cycle.

The advantages, in terms of fuel consumption, of the hybridization are different for different driving cycles; the major benefits are observed for low average speed driving cycles, with many accelerations, decelerations and stops, which can benefit the most from the electric subsystem.

To shed light on the expected variations of vehicle performances, depending on its mission, Figure 12 has been built, simulating several driving cycles and calculating their fuel consumptions: Artemis Urban, FTP75, WTLC Low 1, WLTC Class 1 and WLTC Medium 1 test driving cycles were simulated.

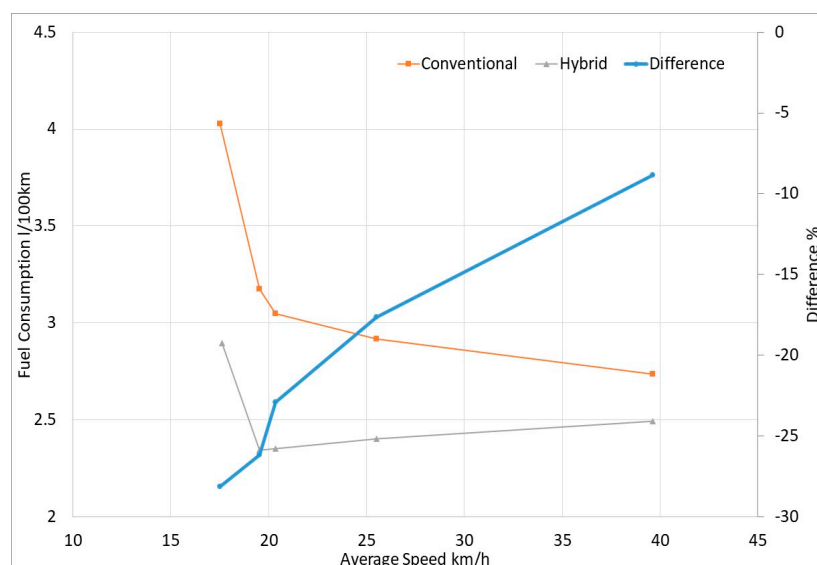


**Figure 12.** Fuel consumption of the conventional microcar and the hybrid version for different driving cycles with different average speeds.

Both conventional and hybrid versions show a broadly acknowledged decrease in fuel consumption with speed (at lower speeds) [23], passing from 4.03 to 2.7 L/100 km for speeds of 17.5 and 39.6 km/h, reducing the value by about 32% compared to the conventional vehicle. The hybrid one shows a reduced speed influence, by about 16%. A comparison between the two powertrains shows a consumption reduction variable with speed, up to 28% at lower speeds, where the electric subsystem gives its best benefits, and decreasing with higher speeds, up to 8% at high average speeds, where the support of the electric motor becomes less important.

#### 4. Hybrid Storage Model

The aging of the batteries depends mainly on the State of Charge (SOC), the battery temperature and the current.

The advantage of the adoption of the UCs is to limit the maximum currents from and to the battery, in order to decrease its internal temperature. The internal power loss, related to the heat source of a cell, is:

$$P_{Loss} = R \cdot I^2 \quad (8)$$

So, it is evident that limiting the maximum current is a good strategy for increasing the life of a battery.

The algorithm proposed implies that the battery supplies a value of power proportional to a mobile averaged value of the power requested by the electric motor, while the UCs are used for the transients.

$$P_{Batt} = P_{avg*} \quad (9)$$

$$P_{SC} = P_{el} - P_{avg*} \quad (10)$$

The  $P_{avg*}$  is the mobile averaged electric power requested. It is calculated by:

$$P_{avg*}^{t+dt} = P_{avg*}^t + \frac{(P_{ist}^{t+dt} - P_{ist}^t)}{\tau} \cdot dt \quad (11)$$

with  $\tau$  as reference time. Such parameter must be taken into account for the following phenomenon:

The SOC of UCs can never be "0" or "1" during every condition of each driving cycle, because in these cases there is no support in reducing the currents for the onboard battery.

To best fit every driving cycle, the  $\tau$  value must be different during positive and negative power from UCs. These positive and negative values can vary with the SOC, in order to never reach the SOC values 0 or 1.

The time constant then has the form:

$$\tau = f^{\pm}(SOC) \cdot \tau^{ref}$$

with  $\tau^{ref}$  a fixed value of the order of 10 s, and two different functions have been set: one where  $P_{el} > P_{avg}$ , and another for  $P_{el} < P_{avg}$ .

Finally, the  $f^{\pm}$  has the following form: when the power from UCs is positive, the  $f^+$  has a linear decreasing behavior with the SOC, as in Figure 13; with longer time constants, the increasing power rate of the battery is lower, and more power and energy are required from the UCs, while if the time constant is lower the battery power reaches more quickly the  $P_{ist}$  value, and less energy and power are required from the UCs.

$$P_{ist} > P_{avg* \rightarrow f^+} \quad (12)$$

$$P_{ist} < P_{avg* \rightarrow f^-} \quad (13)$$

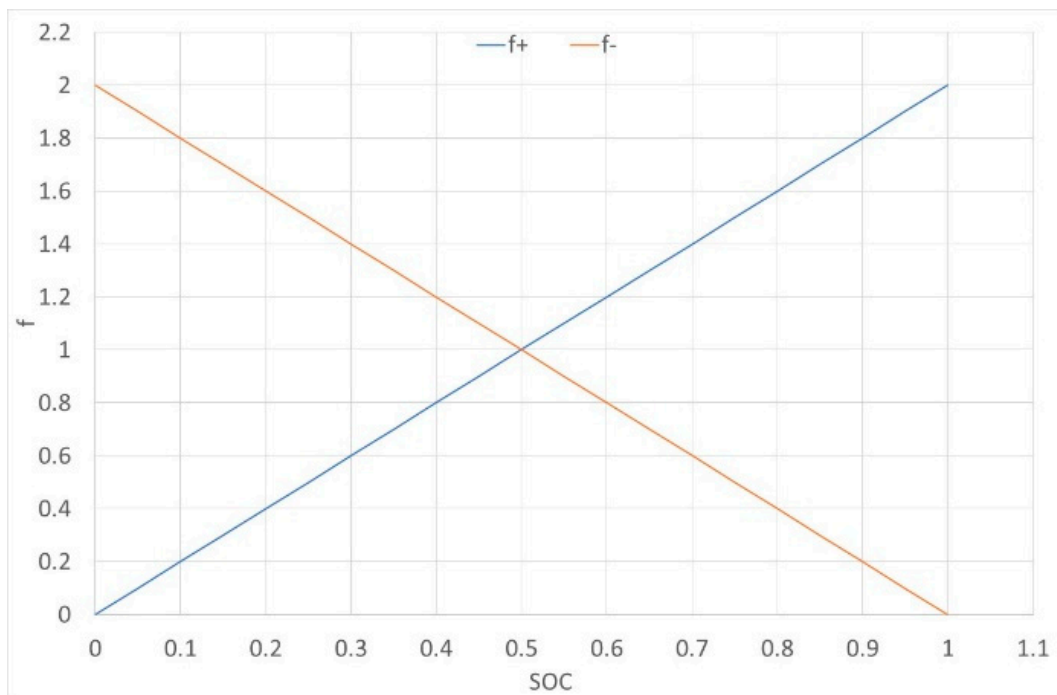


**Figure 13.** Functions curve for the State of Charge.

When  $P_{ist} < P_{avg}$  instead, lower time constants allow more energy recovery for the battery, and higher values allow more recovery for the UCs. In Figure 13, the  $f^{\pm}$  functions vary from 2 at their maximum value to 0 at their minimum.

A last step for avoiding useless energy consumption from UCs is realized when the vehicle stops: with an electric power null or equal to the auxiliary power, the  $P_{avg*}$  becomes immediately zero or equal to the auxiliaries. Without this correction, the present model has a non-negligible consumption at idle, in which the UCs supply power to the auxiliaries until  $P_{avg*} = P_{ist}$  or, due to the fact that  $P_{avg*}$ , reach the stationary value after some seconds.

In Figure 14, the battery power (red line) can be compared with the total electric power (blue line): the smoothed behavior of the battery has halved its maximum value, and the UCs follow the transients of the driving cycle.

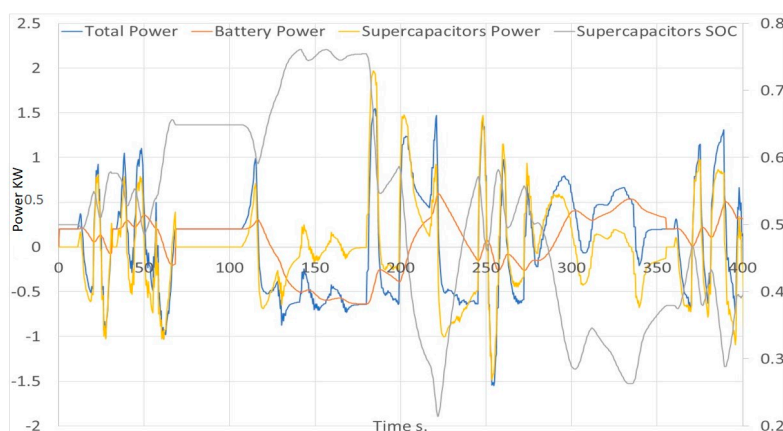


**Figure 14.** Simulated electrical power requested, battery and UCs power during the WLTC Class 1 driving cycle for the hybrid vehicle.

To calculate the battery temperature, the first law of thermodynamics is applied:

$$C_T \cdot \frac{dT_{Cell}}{dt} = P_{Loss} - \frac{(T_{Cell} - T_a)}{R_T} \quad (14)$$

where  $C_T$  is the cell thermal capacitance, set in this work to 281.9;  $R_T$  is the thermal resistance, set to 5.54; and  $T_a$  is the ambient temperature (293 K).

The temperature profiles (Figures 15 and 16) is affected by the different behavior of the current, and the difference is quite high: in the Artemis Urban driving cycle, the temperature rises by about 20 degrees from the start of the cycle, while with the hybrid storage the difference is only 5. The FTP75 urban rises 7 degrees versus about 1, and the WLTC Class 1 driving cycle rises 5 versus about 1.

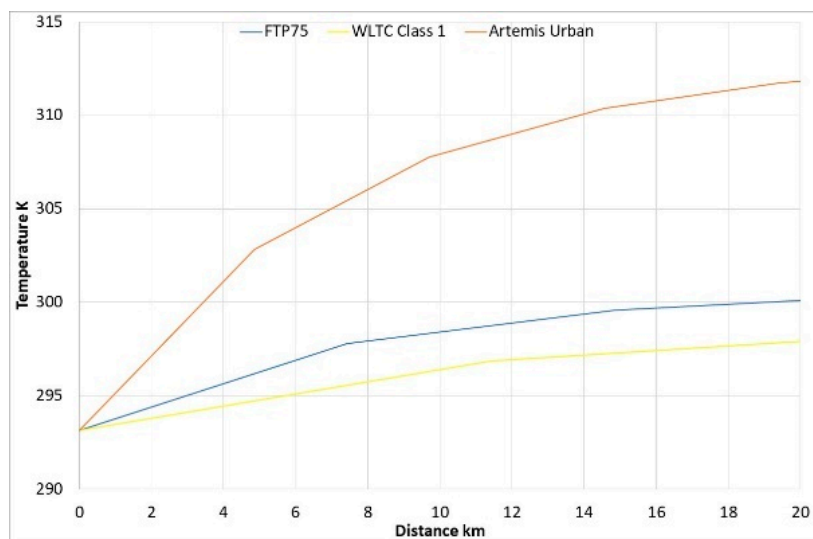


**Figure 15.** Temperature of the battery for the Artemis Urban, FTP75 and WLTC Class 1 with the standard battery.

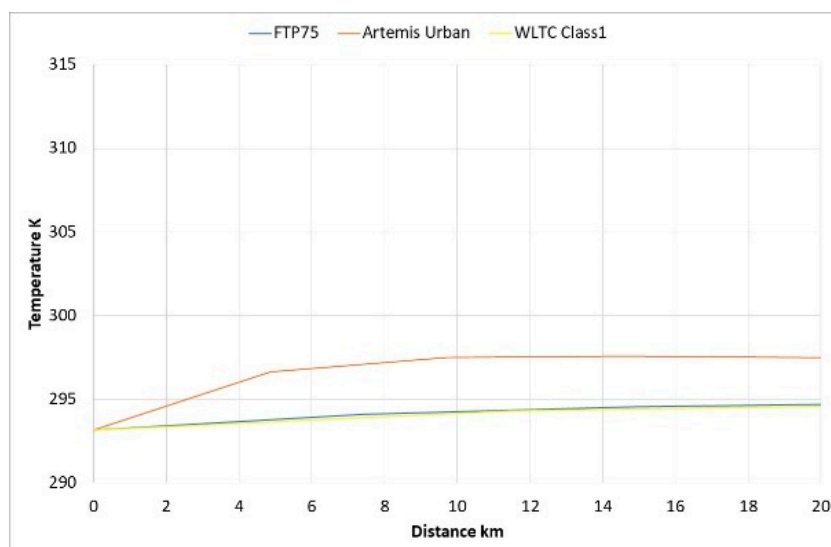


**Figure 16.** Temperature of the battery for the Artemis Urban, FTP75 and WLTC Class 1 with the hybrid storage.

These input data can be then used to calculate the degradation of the battery, and to quantify the benefits of the adoption of the hybrid storage in terms of cycle life.

## 5. Cycle Life Predictions

The battery degradation is mainly a function of its temperature, the SOC and the value of positive or negative current.

Among several studies on how the battery degrades during an unsteady profile usage, in the present work the model proposed by [21] has been used. The model starts from the Dakin degradation model, and has the following form:

$$\frac{dC}{dt^\alpha} = -k \cdot C^n \quad (15)$$

$$k = k(T, SOC, I) = e^{\frac{-b}{aT}} \cdot e^{\frac{c \cdot SOC}{a}} \cdot e^{\frac{d}{a}} \cdot e^{(\frac{a_3}{aT} + b_3)} \cdot \frac{I}{I_0} \quad (16)$$

The exponent “ $n$ ” is unity, and the degradation ratio can be:

$$\frac{C}{C_0} = e^{-k \cdot t^\alpha} \quad (17)$$

Further details can be found in [21], while the coefficients used in the present work are the same as those used for the LG Chem 5.3 Ah. The only modification made was a normalization of the current, imposing  $I_0$  equal to the battery capacity, so for the same battery  $C$  rate the cells used in the present work (the EIG 020 Ah) experience the same degradation as the LG.

The resistance degradation has been neglected in the present work, but for hybrid powertrains it is quite important, due to the fact that the internal resistance rise causes a decrease of the maximum power of a cell; a critical parameter for the batteries of hybrid powertrains.

In Figure 17, it can be observed that the increased life, with or without the UCs, for three different driving cycles varies from more than 70% to more than 170%, and this value is a function of the travel distance only for the shorter travels. For trips longer than 5 km, the advantages reach the stationary value. In the first part of the curve, the difference is due to the presence of many accelerations and power peaks that increase the currents and temperatures, and can be controlled using the battery and UCs. The effect of the driving cycles can be observed in Figure 18: by increasing the transients and the power, the capacity degradation is increased for both standard and hybrid ESS, but the last one shows a better performance as regards the battery life.

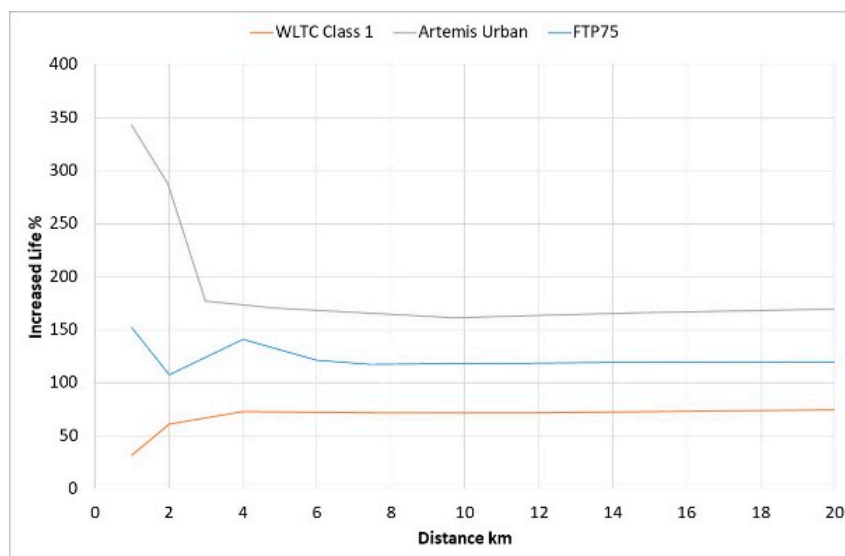
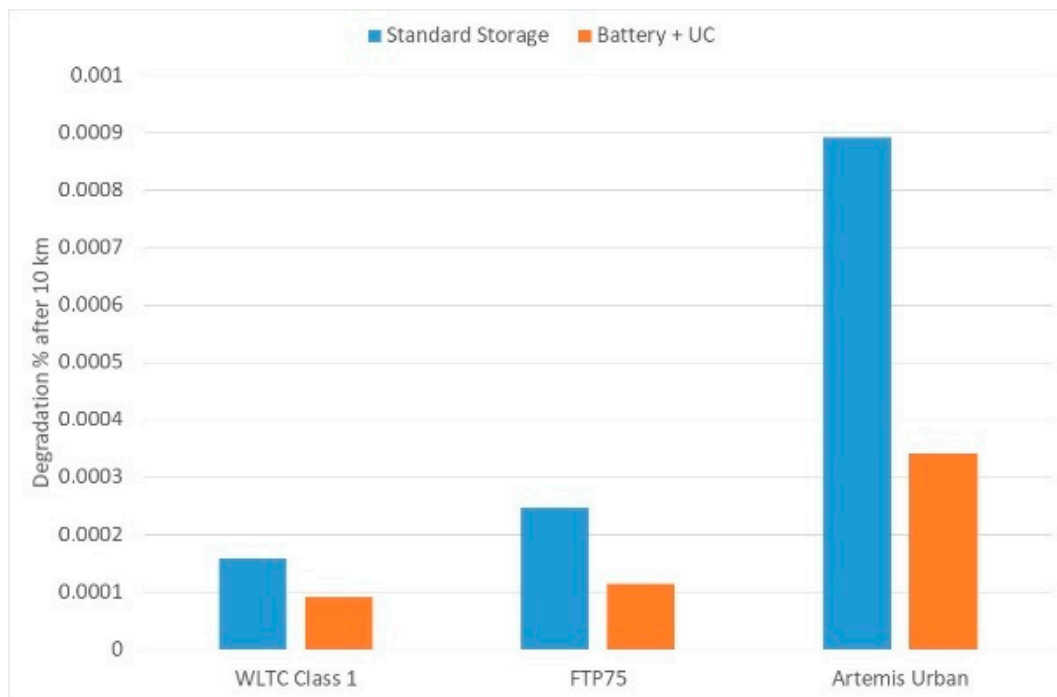


Figure 17. Increased life% with varying the mission distance for different driving cycles.





**Figure 18.** Absolute degradation for different driving cycles after 10 km, with and without UCs.

The comparison between the standard LiBs ESS and a hybrid LiBs/UCs ESS is made with the hypothesis that the trip length is 10 km, while the reference ambient temperature is 293 K and the average SOC is 0.5. The influence of the driving cycle, the SOC and the ambient temperature are analyzed and then discussed.

The influence of the SOC range is shown in Figure 19, which reports the values of degradation in % after 10 km with the WLTC driving cycle, for three different SOC ranges: between 0.3 and 0.7 (with an average value of 0.5), between 0 and 0.4 (with an average value of 0.2) and between 0.6 and 1 (with an average value of 0.8). The degradation increases with the SOC, and also in this case the hybrid storage system performs better than the sole battery storage. In Figure 20, the variation of the battery degradation with the ambient temperature is reported. There is an optimal temperature value around 293 K, while for lower and higher values the degradation increases. The hybrid storage increases the battery life by more than 50%, except for ambient temperatures of 313 K, where the temperature effect becomes higher than the current effect.

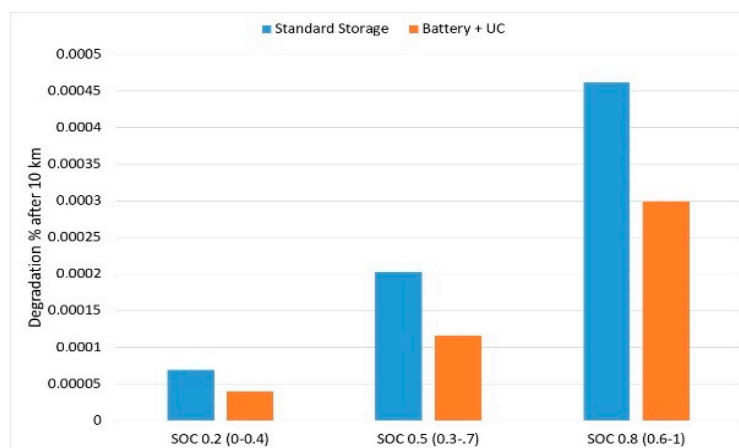


**Figure 19.** Differences between the standard storage and battery with UCs for the WLTC Class 1 with different SOC.

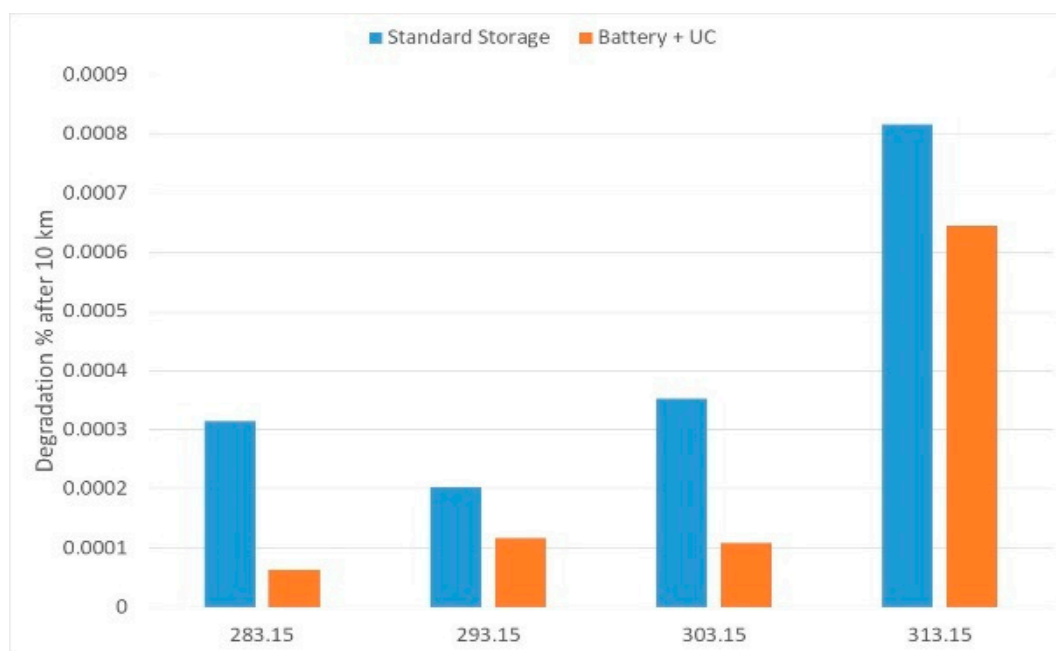


**Figure 20.** Between the standard storage and Battery +UCs during the WLTC Class 1 for different ambient temperature.

## 6. Conclusions

The hybridization of microcars gives many advantages in terms of fuel consumption, pollutants and CO<sub>2</sub> emission. The expected advantages are a function of the driving cycle, expressed in term of average speed and power profile.

The HEV microcar presented in this work also allows the vehicle to run in electric mode at limited speed. Pure electric mode is possible if the engine load requested by the ICE is lower than a threshold value. The threshold is imposed as function of the battery SOC (so that electric traction becomes more and more limited as the SOC goes down).

At higher loads, the ICE normally uses a part of its power output to charge the batteries, this part being a lesser function of ESS SOC.

The benefits of hybridization proved to be functions of the vehicle use. As for the average speed, at the lowest values (17 km/h) the fuel reduction was up to 28% (in the Artemis Urban driving cycle), and decreased up to 8% if the average speed increased to 39 km/h. In the WLTC Class 1 driving cycle, the reduction was 17.7%, and in the first low speed part was 23%.

The adoption of hybrid storages showed its capability in reducing both the maximum current output and temperature of the LiBs: about 50% of current reduction and up to 20 degrees of temperature in the Artemis a driving cycle (the cycle that requires more power than the others).

In terms of LiBs life, the main parameters that influence their degradation are SOC, temperature and current output. HEV control strategies should therefore also consider that higher mean SOC and mean current output values degrade the battery faster. The battery temperature influences the capacity fade, and there is an increase with both high and low temperatures. The adoption of a hybrid storage proved to produce expected benefits in all these cases (ambient temperature, SOC and driving cycles), and the benefits are between 40% and 60% in terms of increased life of the battery.

As future developments, the Hybrid Power Pack will be tested on a test bench, and also an evaluation of the effectiveness and the robustness will be made.

**Author Contributions:** Conceptualization, F.O., C.V.; software, F.O. and C.V.; validation, N.A., M.P. and F.O.; writing—original draft preparation, F.O.; writing—review and editing, N.A., C.V. and M.P.; project administration, F.O. All authors have read and agreed to the published version of the manuscript.

**Funding:** This research was funded by Italian Ministry for Economic Development (MISE), program agreement MISE-ENEA 2016–2018.

**Conflicts of Interest:** The authors declare no conflict of interest.

### List of Acronyms

BEV	Battery Electric Vehicle
CVT	Continuously Variable Transmission
DC	Direct Current
EOL	End Of Life
ESS	Energy Storage System
FTP75	Federal Test Procedure 75
HPP	Hybrid Power Pack
HEV	Hybrid Electric Vehicle
ICE	Internal Combustion Engine
IR	Internal Resistance
ISFORT	Italian Higher Education and Research Institute for Transport
LiB	Li-Ion Battery
NMC	Nickel Manganese Cobalt
SOC	State of Charge
TTW	Tank-To-Wheel
UC	UltraCapacitor
WLTC	Worldwide harmonised Light Vehicles Test Cycle
WTT	Well-To-Tank
WTW	Well-To-Wheel

### References

1. ANCI. 2016. Available online: <http://www.anci.it/mobilita-sostenibile-ricerca-anci-nelle-citta-serpentoni-di-auto-vuote-ma-cala-inquinamento/> (accessed on 1 June 2020).
2. ISFORT. 16° Rapporto Sulla Mobilità Degli Italiani, Roma, 27/11/2019. Available online: [https://www.isfort.it/wp-content/uploads/2019/12/16\\_Rapporto\\_Audimob.pdf](https://www.isfort.it/wp-content/uploads/2019/12/16_Rapporto_Audimob.pdf) (accessed on 16 December 2019).
3. Available online: [https://www.repubblica.it/economia/2016/07/08/news/le\\_macchine\\_in\\_citta\\_girano\\_vuote\\_con\\_2\\_passeggeri\\_si\\_risparmierebbero\\_360\\_milioni-143682470/](https://www.repubblica.it/economia/2016/07/08/news/le_macchine_in_citta_girano_vuote_con_2_passeggeri_si_risparmierebbero_360_milioni-143682470/) (accessed on 1 June 2020).
4. Villante, C.; Anatone, M.; De Vita, A.; Ortenzi, F.; Ursitti, E.M. *A New Parallel Hybrid Concept for Microcars: Propulsion System Design, Modeling and Control*; SAE Technical Paper 2019-24-0246; SAE: Warrendale, PA, USA, 2019.
5. Barsali, S.; Pasquali, M.; Pedè, G. *Definition of Energy Management Technique for Series Hybrid. Vehicles*; EVS: Pusan, Korea, 2002.
6. Ortenzi, F.; Pedè, G.; Rossi, E. *Cycle Life Cost Assessment of a Hybrid Lead Acid Battery-Supercapacitor Storage for an Electric Microcar*; SAE Technical Paper 2014-01-1816; SAE: Warrendale, PA, USA, 2014.
7. Ortenzi, F.; Pedè, G.; Rossi, E. Lithium-Ion/Supercapacitors storage system powered microcar: Development and testing. *Energy Procedia* **2015**, *81*, 422–429. [[CrossRef](#)]
8. Conte, M.; Genovese, A.; Ortenzi, F.; Vellucci, F. Hybrid battery-supercapacitor storage for an electric forklift: A life-cycle cost assessment. *J. Appl. Electrochem.* **2014**, *44*, 523–532. [[CrossRef](#)]
9. Solera, L.; Puccetti, A.; Pennese, M. Inductor tied Ultracapacitor Module devoted to 12V Battery Starter Alternator Systems. In Proceedings of the Global Powertrain Congress 2007, Berlin, Germany, 17–19 June 2007.
10. Zhang, C.; Wang, D.; Wang, B.; Tong, F. Battery Degradation Minimization-Oriented Hybrid Energy Storage System for Electric Vehicles. *Energies* **2020**, *13*, 246. [[CrossRef](#)]
11. Zhang, Q.; Deng, W.; Zhang, S.; Wu, J. A Rule Based Energy Management System of Experimental Battery/Supercapacitor Hybrid Energy Storage System for Electric Vehicles. *J. Control. Sci. Eng.* **2016**, *2016*, 6828269. [[CrossRef](#)]
12. Pugi, L.; Alessandrini, A.; Barbieri, R.; Berzi, L.; Pierini, M.; Cignini, F.; Genovese, A.; Ortenzi, F. Design and Testing of a Supercapacitor Storage System for the Flash Recharge of Electric Buses. *Int. J. Electr. Hybrid. Veh.* Accepted.

13. Jongerden, M.R.; Haverkort, B.R. *Battery Modeling*; Technical Report TR-CTIT-08-01; University of Twente, Centre for Telematics and Information: Oslo, Norway, 2008.
14. ISO 12405–2012. Electrically Propelled Road Vehicles—Test Specification for Lithium-Ion Traction Battery Packs and Systems—Part 2: High-Energy Applications. Available online: <https://www.iso.org/standard/55854.html> (accessed on 15 June 2020).
15. Cignini, F.; Ortenzi, F.; Rossi, E.; Virginio, S. Spazia-HPP: Hybrid plug-in for small vehicle. *Energy Procedia* **2015**, *81*, 108–116. [[CrossRef](#)]
16. Ortenzi, F.; Vesco, E. *An Improved Multi-Pipe Junction Model for Engine Thermodynamic and Gas Dynamic Simulations*; SAE Technical Paper 2013-24-0069; SAE: Warrendale, PA, USA, 2013. [[CrossRef](#)]
17. Ortenzi, F.; Genovese, A.; Carrazza, M.; Rispoli, F.; Venturini, P. *Exhaust Energy Recovery with Variable Geometry Turbine to Reduce Fuel Consumption for Microcars*; SAE Technical Paper 2018-01-1825; SAE: Warrendale, PA, USA, 2018.
18. Baghdadi, I.; Briat, O.; Delétage, J.Y.; Gyan, P.; Vinassa, J.M. Lithium battery aging model based on Dakin's degradation approach. *J. Power Sources* **2019**, *325*, 273–285. [[CrossRef](#)]
19. Villante, C.; Rossi, E. A Hybrid City Car. *IEEE Veh. Technol. Mag.* **2011**, *6*, 24–37. [[CrossRef](#)]
20. Available online: <https://www.heinzmann-electric-motors.com/en/downloads/pms-disc-motors/pms-100> (accessed on 15 June 2020).
21. Grün, T.; Doppelbauer, M. Comparative Concept Study of Passive Hybrid Energy Storage Systems in 48 V Mild Hybrid Vehicles Varying Lithium-Ion Battery and Supercapacitor Technologies. *World Electr. Veh. J.* **2019**, *10*, 71. [[CrossRef](#)]
22. Winterbone, D.E.; Pearson, R.J. *Theory of Engine Manifold Design*; Professional Engineering Pub.: London, UK, 2000.
23. Sobrino, N.; Monzon, A.; Hernandez, S. Reduced Carbon and Energy Footprint in Highway Operations: The Highway Energy Assessment (HERA) Methodology. *Netw. Spat. Econ.* **2016**, *16*, 395–414. [[CrossRef](#)]



© 2020 by the authors. Licensee MDPI, Basel, Switzerland. This article is an open access article distributed under the terms and conditions of the Creative Commons Attribution (CC BY) license (<http://creativecommons.org/licenses/by/4.0/>).